Viscous cavity damping of a microlever in a simple fluid

A. Siria[1,2], A. Drezet[1], F. Marchi[1,3], F. Comin[3], S. Huant[1] and J. Chevrier[1]
[1] *Institut Néel, CNRS and Université Joseph Fourier Grenoble, BP 166 38042 Grenoble Cedex 9, France*
[2] *CEA/LETI-MINATEC, 17 Avenue des Martyrs 38054 Grenoble Cedex 9, France*
[3] *ESRF, 6 rue Jules Horowitz 38043 Grenoble Cedex 9, France*

We consider the problem of oscillation damping in air of a thermally actuated microlever as it is gradually approached towards an infinite wall in parallel geometry. As the gap is decreased from 20 μm down to 400 nm, we observe the increasing damping of the lever Brownian motion in the fluid laminar regime. This manifests itself as a linear decrease with distance of the lever quality factor accompanied by a dramatic softening of its resonance, and eventually leads to the freezing of the CL oscillation. We are able to quantitatively explain this behavior by analytically solving the Navier-Stokes equation with perfect slip boundary conditions. Our findings may have implications for microfluidics and micro/nano-electromechanical applications.

PACS numbers: 47.61.Fg, 47.15.Rq, 85.85.+j, 07.79.Lh

Micro- and nano-scale mechanical levers are increasingly used as sensors and actuators in a large variety of fundamental studies and applications. Mass detection at the zeptogram scale [1], sub-attonewton force detection [2] and optical cooling of microlevers [3] are among the most spectacular achievements of oscillating cantilevers (CLs). These realizations mainly rely upon the extraordinary high quality factors (Q) of oscillating CLs in vacuum and/or cryogenic temperatures where values exceeding 100 000 are attainable. Clearly, maintaining such performances in air or in a liquid is a very challenging issue as oscillation damping in the surrounding fluid dramatically degrades Q. This has been partially circumvented by using ultrasmall self-sensing nano-electromechanical systems (NEMS, *i.e.*, actuated mechanical devices made from submicron mechanical components facing each other) operating in ambient conditions of temperature and pressure [4].

However, oscillating CLs are also used in viscous environments on many occasions [5, 6, 7, 8]. In Atomic Force Microscopy (AFM) for example, a resonant CL is used to measure surface topography and physico-chemical properties of various materials not only in air but also in liquids [9] for, *e.g.*, visualizing dynamic biomolecular processes at video rate [10]. The interaction between an AFM CL and a surrounding liquid has been used for a distance calibration in a Casimir force measurement [11] and has led very recently to the spectacular demonstration of a repulsive Casimir force [12]. Therefore, the need for a quantitative study of the CL behavior in viscous micro- and nano-scale environments is increasing. In this letter, we report such a quantitative study and show, down to the submicron scale and in the demanding plane-plane geometry, how confinement and boundary conditions at the solid-fluid interfaces conspire to change the coupling to thermal bath and how this can freeze out the lever oscillation.

When a CL beam vibrates in a viscous fluid, the fluid offers resistance to the beam displacement [13, 14]. If the CL is vibrating close to a solid surface, the behavior of the fluid and, consequently, that of the lever are modified by the surface due to confinement. The Navier-Stokes (NS) equations give a complete description of the fluid behavior taking into account the particular environment under analysis. However an analytical solution of NS equations is possible only for a restricted number of geometries and comparison of theory with experimentally relevant configurations is in general a complex matter or is even lacking, especially at the deep micron and submicron scales [15, 16, 17, 18, 19, 20] where boundary conditions at the fluid-solid interfaces are strongly modified [21, 22, 23, 24]. In this work, we focus on the dynamical behavior of a microlever close to a planar rigid surface in the air. Provided that adapted boundary conditions are used, the NS equations can be solved analytically for this plane-plane model geometry that mimics a basic part of a MEMS (the counterpart of a NEMS in the micron

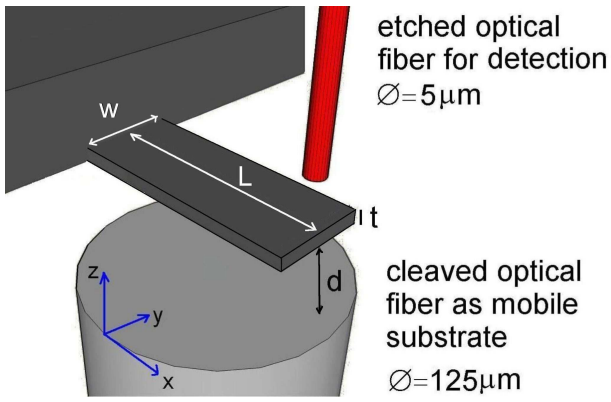

FIG. 1: Scheme of the experimental setup (not to scale). The analyzed mechanical system is a standard AFM CL. A cleaved optical fiber (bottom) is used as mobile substrate forming a cavity with the CL. An etched optical fiber (top) is used for the interferometric detection of the CL Brownian motion. The main geometrical parameters used in the text are identified, the z origin is taken on the flat cleaved-fiber surface.

range) device operating in the air. This, combined with the use of the fluctuation-dissipation theorem and of an experimental arrangement specially designed to gain access to the intrinsic behavior of the CL, enables us to make a quantitative comparison between theory and experiment in a wide range of cavity lengths down to a few hundreds of nanometers.

Our setup is shown schematically in Fig. 1. Its first specification is that the CL - a commercial thin silicon AFM CL [25] for liquid imaging with dimensions $L \times w \times t = 107 \times 30 \times 0.18\ \mu m^3$ - is actuated by the stochastic thermal noise only. This induces sub-Angstrom oscillations at the CL resonance frequency ($\omega_0/(2\pi) \simeq 49.5$ kHz), thereby allowing us to consider the fluid in the cavity in the laminar regime. Second, the planar rigid surface facing the CL to form a parallel-plate cavity is made of a cleaved optical fiber with a diameter of 125 μm that is mounted over a three-axis inertial motor so as to be able to *adjust the cavity gap*. This positioning system offers a large displacement range (8 mm each axis full range) with a good accuracy (40 nm per step). Finally, the CL Brownian motion is measured by means of a *non invasive* interferometric detection based on the use of a very thin optical fiber facing the CL at a 2 μm distance. This fiber has been chemically etched so as to reduce its diameter to 5 μm. This corresponds basically to the fiber core diameter plus a residual amount of the optical cladding for better light guidance. The large ratio in excess of 600 between the areas of the cleaved and detection fibers insures that only the cleaved one induces air confinement, not the etched one, which is used for detection purpose only. Therefore, no additional uncontrolled confinement and damping are produced by the detection fiber.

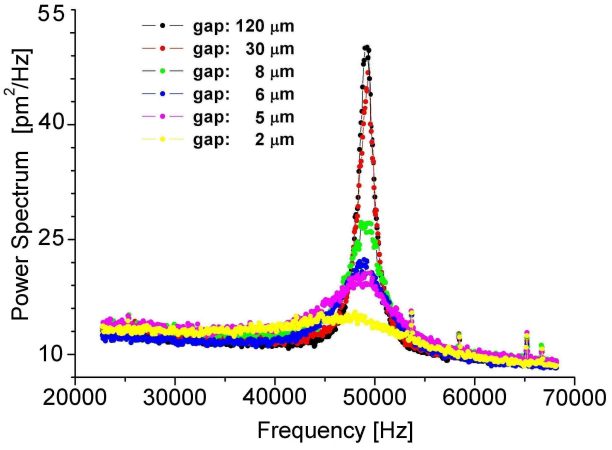

FIG. 2: The experimental Brownian oscillation power spectrum of the microlever for different cavity gaps.

An AFM CL vibrating in a viscous fluid may be viewed as a driven and damped 1D harmonic oscillator whose equation of motion reads

$$m\ddot{z}(t) + \gamma\dot{z}(t) + kz(t) = F_{ext}, \tag{1}$$

where m, $z(t)$, k are the CL effective mass, time-dependent position, and stiffness, respectively, γ is the damping factor and F_{ext} the external (*i.e.*, thermal) driving force. According to the fluctuation-dissipation theorem, the thermal Brownian motion of the CL at temperature T is accounted for by a frequency independent force power spectrum defined as $S_F(\omega) = 2k_BT\gamma$ (k_B is the Boltzmann constant, ω the pulsation linked to the frequency $f = \omega/(2\pi)$). Starting from Eq. 1 we obtain the CL displacement power spectrum as $S_z(\omega) = S_F(\omega)|\chi(\omega)|^2$, where the CL transfer function $\chi(\omega)$ is given by:

$$\chi(\omega) = \frac{1}{m\left(\omega_0^2 - \omega^2\right) - i\gamma\omega} \tag{2}$$

with $\omega_0 = \sqrt{\frac{k}{m}}$. In the limit of small damping, *i.e.*, $\frac{\gamma}{m} \ll \omega_0$, $S_z(\omega)$ has a resonance at ω_0.

In Fig. 2, the experimental Brownian oscillation power spectrum $2S_z(\omega)$ is presented as a function of frequency f for different cavity gaps d. It is clearly seen that the resonance peak dramatically broadens and softens to lower frequencies with decreasing gap. Within the experimental accuracy, we find that the area under the resonance curves in Fig. 2 remains constant and equals to the thermal energy. This shows that the CL damping increases with decreasing gap.

Now, we turn on to a quantitative analysis of the experiment. The fluid responsible for the CL damping is the air confined between the CL and the mobile fiber. The dynamic of such an incompressible fluid is described by the NS equations

$$\rho\left[\frac{\partial\vec{v}}{\partial t} + \vec{v}\cdot\nabla\vec{v}\right] = \eta\nabla^2\vec{v} - \nabla p, \tag{3}$$

where $\vec{v}$ is the fluid velocity, ρ its density, η its dynamical viscosity and p the gas pressure. In the laminar regime, *i.e.*, in the limit of small Reynolds numbers, Eq. 3 simplifies to $\eta\nabla^2\vec{v} \simeq \nabla p$. In order to solve the NS equations, one needs to know the specific boundary conditions existing at the fluid-solid interfaces (for simplicity we assume the cavity plates to be infinitely extended). While for macroscopic hydrodynamic applications one usually accepts that fluids do not slip against solid walls, this is generally not true for microfluidic problems involving MEMS or NEMS [21]. A critical parameter in this respect is the Knudsen number [21] $K_n = \bar{\lambda}/d$ which depends on the gas mean free path $\bar{\lambda}$. For air at ambient conditions $\bar{\lambda} \simeq 60$ nm which leads here to $K_n \sim 0.001 - 0.06$. In this range of K_n values, it is already known that fluid-slip can occur over a solid interface [21, 22, 23]. In particular, partial fluid-slip has been recently observed in the plane-sphere geometry in air using an AFM in dynamic mode [24]. However, none of the previous works investigated the regime of Brownian oscillations with typical CL amplitudes $\delta z \sim 0.05$ nm much smaller than $\bar{\lambda}$ (*i.e.*,

$\bar{\lambda}/\delta z \sim 10^3$). In such a regime, boundary conditions are expected to be even more strongly modified [21] compared with the macroscopic regime although it is not yet known how much they are modified. Here, we make the hypothesis of perfect slip, historically anticipated by Navier [26], for which friction along the solid interface is prohibited, and show that we can obtain a consistent quantitative description of our experimental data. This hypothesis results in a velocity gradient along the z direction which leads to a Stokes friction coefficient:

$$\gamma = \frac{2\eta A}{d}, \tag{4}$$

where $A = wL$ is the cantilever surface. The usual no-slip condition at the fluid solid interface would predict $\gamma \simeq \eta w L^3/d^3$, in clear disagreement with the experiment. As a direct consequence, Eq. 4 leads to a much smaller decay of the friction force with d than predicted usually. Quantitative information on the damping factor is obtained from the analysis of the CL quality factor. Both quantities are linked together by the relation $Q = \frac{k}{\omega_0 \gamma}$, which becomes for small gaps:

$$Q = \frac{k}{2\omega_0 \eta A} d. \tag{5}$$

Eq. 5 predicts a linear dependence of Q with d that can be compared with experiment.

Fig. 3 depicts the quality factor as function of the cavity gap. Two different regimes can be distinguished. For large gaps above 40 μm, the quality factor remains constant. This is the unconfined fluid regime where no additional damping can take place with decreasing gap. For smaller gaps however, the quality factor tends to decrease with a decreasing gap. We will focus below on the small gap regime where the hypothesis of infinite planes is physically justified. Since the AFM CL has a surface 10 times smaller than the substrate fiber, the gap limit for the hypothesis of infinite planes to remain physically sound can be estimated by taking the apparent CL surface as reference, *i.e.* $d_{\text{lim.}} \approx 15\mu m$.

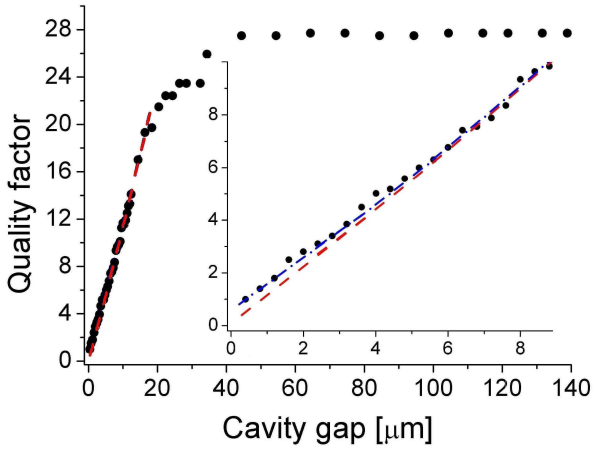

FIG. 3: The quality factor as a function of the cavity gap. The black dots are the experimental points. The insert depicts a zoom of the small gap range. In both cases, the red curves exhibit the theoretical prediction based on Eq. 5, *i.e.*, the prediction of the NS equation in the perfect parallel plate geometry. The blue dash-dotted line in the insert shows the prediction of the NS model taking into account a residual angular misalignment of the cavity as discussed in the text.

As shown in the inset of Fig. 3 the experimental results and the theoretical prediction of Eq. 5, with no adjustable parameter [27], coincide to within 5% for gaps larger than 5 μm but for smaller separations, the agreement worsens to reach 100% at the smallest gap, 400 nm. We interpret this difference with a residual small angular misalignment of the two facing parallel plates. For small misalignment, the problem can be treated within an approximation similar to the Proximity Force Approximation (PFA) used, for instance, in the Casimir force formulation in the sphere-plane geometry [28]. In this approximation, the corrected damping factor becomes:

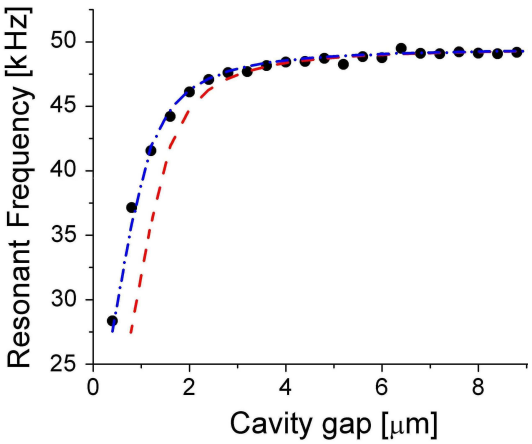

FIG. 4: The resonance frequency as function of the cavity gap in the small gap regime. Like in Fig.3, the red dashed, respectively blue dash-dotted curves is the prediction of the NS model for the perfectly aligned, respectively slightly misaligned, cavity.

$$\gamma = \int_0^L \int_0^w 2\eta \frac{dx \cdot dy}{d_0 + x\tan\alpha + y\tan\beta} \tag{6}$$

where d_0 is the shortest distance from the inclined CL to the substrate, α and β are the lateral tilt angles of the CL with the mobile surface in the x and y directions, respectively. The angle values that permit to reproduce the evolution of the disagreement between experiment and theory, as presented in Fig. 3, are $\alpha \approx \beta \approx 10\ mrad$. Considering these misalignment angles, the good agreement between theory and experiment can now be extended down to the smallest gap range that we have measured as can be seen in Fig. 3. Over the entire range 400 $nm - 15\ \mu m$, the remaining disagreement is $\approx 5\%$ only [29].

We now discuss the frequency softening of the CL oscillation, the other salient experimental fact revealed by Fig. 2. In the limit of large damping, *i.e.* the approximation $\frac{\gamma}{m} \ll \omega_0$ no longer holds, the power spectrum of Eq. 2 has a down-shifted resonance pulsation ω' given by:

$$\omega' = \sqrt{\omega_0^2 - \frac{1}{2}\left(\frac{\gamma}{m}\right)^2} \tag{7}$$

Fig. 4 shows that the resonance frequency shift $(\omega' - \omega_0)/(2\pi)$ can be extremely large. One step further below $400nm$, a complete freezing of the CL oscillation would have been observed. This was precluded by the residual angular misalignment discussed above. Taking into account for data analysis of the misalignment obtained from Fig. 3, we can quantitatively model the measurements in Fig. 4 without any adjustable parameter whatsoever. Therefore, beside the CL width that governs the Q factor behavior at large scale (Fig. 3), another shorter characteristic length is here emphasized in the submicron range, i.e. $d_{\text{crit.}} = \frac{\sqrt{2}\eta}{m}\frac{A}{\omega_0}$ (around 500 nm in our case), which is the gap width cancelling the resonance frequency in Eq. 7. This characteristic length is determined by the CL dynamics and the fluid viscosity.

In conclusion, we have presented high sensitivity measurements of the damping of a thermally driven CL in a simple fluid confined in a microcavity formed by this CL facing an infinite wall. As the cavity length decreases, the fluid confinement induces a dramatic damping of the CL Brownian motion which can lead to its complete freezing at small gaps. A consequence of our work is that micro- or nano-oscillators can either present high Q factors or be overdamped systems depending on their actual geometry, resonance frequency, oscillator substrate gap and, of course, ambient viscosity. These findings may impact the design of modern NEMS and microfluidic devices since the $1/d$ dependence strongly reduces dissipation even for separations d as large as thousands of mean free path $\bar{\lambda}$ (see Fig. 3). This $1/d$ behavior can be furthermore described by solving the Navier-Stokes equation with perfect solid-fluid slip boundary conditions. The agreement between experiment and our model is found over a broad range of cavity lengths, including the submicron range. Interesting extensions of the present work include the study of parameters affecting boundary conditions, such as external actuation of CLs (to obtain large oscillation amplitude) [30], nanostructuration [4], and surface chemical properties [8].

We are grateful to Giovanni Ghigliotti for helpful discussions. Our thin etched optical fiber has been prepared by Jean-Francois Motte. This research was partly supported by a "Carnot-NEMS" collaborative grant between CEA-LETI and Institut Néel.

[1] Y. T. Yang, *et al.*, Nano Lett. **6**, 583 (2006).
[2] H. J. Mamina and D. Rugar, Appl. Phys. Lett. **79**, 3358 (2001).
[3] K. Karrai, Nature (London) **444**, 41 (2006); C. Metzger, *et al.*, Phys. Rev. Lett. **101**, 133903 (2008); G. Jourdan, *et al.*, Phys. Rev. Lett. **101** 133904 (2008).
[4] Mo Li, *et al.*, Nature Nanotech. **2**, 114 (2007).
[5] C. Cottin-Bizonne, *et al.*, Phys. Rev. Lett. **94**, 056102 (2005).
[6] W. Y. Shih, *et al.*, J. Appl. Phys. **89**, 1497 (2001).
[7] P. K. Hansma, *et al.*, Appl. Phys. Lett. **64**, 1738 (1994).
[8] A. Maali, *et al.*, Phys. Rev. Lett. **96**, 086105 (2006).
[9] A. Raman, *et al.*, Nanotoday **3**, 20 (2008).
[10] T. Ando, *et al.*, Prog. Surf. Science **83**, 337 (2008).
[11] J. N. Munday, *et al.*, Phys. Rev. A **78**, 032109 (2008).
[12] J. N. Munday, F. Capasso, and A. Parsegian, Nature (London) 457, 170 (2009).
[13] L. Bellon, J. Appl. Phys. **104**, 104906 (2008).
[14] R. B. Bhiladvala and Z. J. Wang, Phys. Rev. E **69**, 036307 (2004).
[15] C. P. Green and J. E. Sader, J. Appl. Phys. **98**, 114913 (2005).
[16] T. Naik, *et al.*, Sensor and Actuators A: Physical **102**, 240 (2003).
[17] M. R. Paul and M. C. Cross, Phys. Rev. Lett. **92**, 235501 (2004).
[18] J. Dorignac, *et al.*, Phys. Rev. Lett. **96**, 186105 (2006).
[19] S. Basak, *et al.*, J. Appl. Phys. **99**, 114906 (2006).
[20] R. C. Tung, *et al.*, J. Appl. Phys. **104**, 114905 (2008).
[21] P. Tabeling, *Introduction to microfluidics* (Oxford University Press, USA, 2006).
[22] D. Y. C. Chan, and R. G. Horn, J. Chem. Phys. **83**, 5311 (1985).
[23] O. I. Vinogradova, Langmuir **11**, 2213 (1995).
[24] A. Maali and B. Bhushan, Phys. Rev. E **78**, 027302 (2008).
[25] The CL tip has been removed by focused-ion-beam milling.
[26] S. Goldstein, Ann. Rev. Fluid. Mech. **1**, 1 (1969).
[27] The CL dimensions have been measured by electron microscopy. The air viscosity was taken as $\eta \simeq 1.8 \times 10^{-5} kg/ms$. The CL stiffness $k = 0.0396 N/m$ has been experimentally determined from Fig. 2 using the energy equipartition theorem.
[28] B. V. Derjaguin, *et al.*, Q. Rev. Chem. Soc. **10**, 295 (1956).
[29] Following Ref. [8], the ultra small CL oscillation precludes any mass addition to the lever, in contrast with Ref. [16] where this effect is dominant for actuated macroscopic levers.
[30] R. A. Bidkar, *et al.*, Appl. Phys. Lett. **94**, 163117 (2009).